Elimination of Birefringence Induced Scale Factor Errors in the In-Line Sagnac Interferometer Current Sensor

Shayne X. Short, Josiel U. de Arruda, Alexandr A. Tselikov, and James N. Blake

Abstract— **This paper presents theoretical and experimental results showing the effects of linear and circular birefringence on the sensing coil of an in-line Sagnac interferometer current sensor. Linear birefringence induces local scale factor variations along the length of the sensing coil which can be suppressed with circular birefringence. We show that by winding the sensing coil with tension in a helix configuration, these variations may be effectively reduced to zero for ordinary single mode fiber. In our opinion, this method of implementation overcomes the need to use annealed fiber in the sensing coil.**

Index Terms—**Fiber-optic current sensors, Sagnac interferometer.**

I. Introduction

FIBER-OPTIC current sensors which rely on Ampère's law and the Faraday effect are universally sensitive to changes in the linear birefringence, δ, in their sensing coils. Changing stresses and temperature may change the total δ or its distribution along the sensing coil which in turn changes the evolution of the state of polarization of the light through the sensing coil. This in turn changes the point by point sensitivity of the coil to the magnetic field. The result is that both the scale factor relating the sensor output to the current in the enclosed wire and the isolation of the sensor to currents in nearby wires are subject to errors and changes in real environments [1], [2]. In this paper, we address these errors particularly as they affect the in-line Sagnac interferometer current sensor [3]–[8] shown in Fig. 1. We present theoretical and corroborating experimental results showing how the point by point sensitivity of the sensing fiber varies along its length in the case of a uniformly distributed δ. By integrating over the local sensitivity function, we obtain the overall sensor scale factor. Results for both open and closed-loop operation of the sensor are obtained.

A particular concern is to find a method to desensitize the system against the effects of δ. The use of annealed fibers [9] or specialty low-strain optic coefficient fibers [10] solves the problem, however, it is desirable in practice to avoid these brittle fibers both because of the added handling cost and the loss of the significant advantage the in-line Sagnac interferometer version of the current sensor possesses which is that it can be installed without disconnecting the current carrying wire by simply wrapping the sensing coil around the conductor. We present theoretical and experimental results that explicitly show how adding circular birefringence to the sensing coil stabilizes the scale factor on a point by point basis. Winding the sensing coil under modest tension in a loop helix is demonstrated to add sufficient circular birefringence to an ordinary single-mode fiber to provide for a constant scale factor along the entire length of the sensing fiber.

The scale factor of the in-line Sagnac interferometer is determined both by the quality of the quarter-waveplate and the sensing fiber. For mitigating the errors associated with the use of an imperfect quarter waveplate, we refer the reader to our previous paper [8].

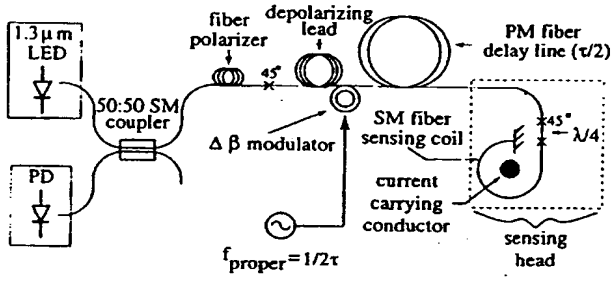

Fig. 1. In-line Sagnac interferometer current sensor.

II. In-Line Sagnac Interferometer Current Sensor

The in-line Sagnac interferometer current sensor (Fig. 1) is a reciprocal device which extracts the Faraday induced phase shift by interfering two orthogonally polarized light waves traveling through the optical circuit in reverse order. These waves travel down the polarization maintaining (PM) fiber delay line linearly polarized and through the sensing head circularly polarized. On the return trip, each of the optical waves ideally assumes the orthogonal sense of polarization at each point in the sensing head and PM fiber delay line. Reciprocal optical effects arising from strains induced by acoustic vibrations and changing thermal environments are cancelled because both beams travel the same optical path [3], [6]. For current sensing applications, the only contributor

Manuscript received July 29, 1997; revised March 26, 1998. This work was supported by the Texas Space Grant Consortium and the Center for Electronic Materials, Devices, and Systems at Texas A&M University. The work of S. X. Short was supported by TU Services Corporate R&D Department of the Texas Utilities Company. J. U. de Arruda was supported by the Instituto de Estudos Avançados (IEAv), S. J. dos Campos, Brazil. The work of A. A. Tselikov was supported by the National Science Foundation under Grant NSF 93-664.

The authors are with the Department of Electrical Engineering, Texas A&M University, College Station, TX 77843 USA.

Publisher Item Identifier S 0733-8724(98)07413-1.

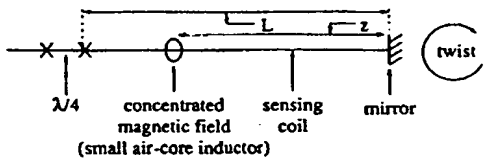

Fig. 2. Straight sensing coil geometry and setup.

to the phase difference between the two beams is that from the Faraday effect, and the total phase shift is $4VNI$ where V is the Verdet constant of the sensing fiber glass, N is the number of turns of fiber around the current carrying wire, and I is the current in the wire. For simplicity, we substitute F for VNI, i.e., $F \equiv VNI$.

III. Mathematical Modeling of the Local Scale Factor

We analyze the spatial variation of the scale factor relating the response of the sensor to a localized magnetic field (Fig. 2). We assume that the total linear and circular birefringences, (δ and $2T$), are uniformly distributed throughout the sensing coil of length L.

In an optical fiber current sensor, the sensing coil is normally wound around the current carrying conductor to utilize Ampère's law in extracting the information of the current. In this case, the magnetic field $\vec{H}$ is integrated all along the loop which consists of an integral number of turns around the conductor. Here, we are interested in the variation of scale factor along the path of integration, namely, along the sensing coil. To model this, we use a Jones matrix analysis assuming a localized magnetic field $\vec{H}$ to be located a distance z from the terminating mirror of the sensing coil. The following parameter definitions are used to simplify the notation:

$$\phi = \left(\frac{L-z}{L}\right) \cdot \sqrt{\delta^2 + (2T)^2} \tag{1}$$

$$\gamma = \left(\frac{z}{L}\right) \cdot \sqrt{\delta^2 + (2T)^2} \tag{2}$$

$$\chi = \tan^{-1}\left(\frac{2T}{\delta}\right) \tag{3}$$

$$P = \cos\left(\frac{\phi}{2}\right) \tag{4}$$

$$Q = \sin\left(\frac{\phi}{2}\right) \cdot \cos\chi \tag{5}$$

$$R = \sin\left(\frac{\phi}{2}\right) \cdot \sin\chi \tag{6}$$

$$X = \cos\left(\frac{\gamma}{2}\right) \tag{7}$$

$$Y = \sin\left(\frac{\gamma}{2}\right) \cdot \cos\chi \tag{8}$$

$$Z = \sin\left(\frac{\gamma}{2}\right) \cdot \sin\chi. \tag{9}$$

The light first travels through the polarizer, $\hat{L}_p$, after which it is aligned to a 45° splice, $\hat{L}_{45°}$, to the polarization maintaining (PM) fiber delay line $\hat{L}_{\mathrm{PMin}}$ which possesses a delay time of $\tau/2$ and a differential polarization delay time of $\Delta\tau$. A birefringence modulator located just before the PM fiber delay line is included within this Jones matrix. This modulator provides the phase difference modulation between the two interfering light waves. As in the fiber optic gyro, the modulator operates at maximum efficiency when the round-trip delay time, τ, and the fundamental modulator frequency, f_p, are related by $f_p = \tau/2$. We modulate the birefringence using a waveform $\psi(t)$ provided by a piezoelectric tranducer (PZT—open-loop case) or an integrated optics modulator (IOM—closed-loop case). After propagating through the delay line, the light then passes through a quarter-waveplate, $\hat{L}_{\lambda/4}$, aligned at 45° with respect to the delay line, $\hat{L}_{45°}$, before entering the sensing coil.

The sensing coil is divided into three sections; two sections having lengths $L - z$ and z which contain only the linear and circular birefringences surround a very short piece of fiber which is subjected to a magnetic field. The matrix $\hat{L}_{\mathrm{coil1}}$ represents the segment of fiber between the quarter-waveplate ($\lambda/4$) and the concentrated magnetic field element, represented by $\hat{L}_{F\mathrm{in}}$. The fiber element between the position of the magnetic field element and the mirror is represented by $\hat{L}_{\mathrm{coil2}}$. We assume all elements are ideal with the exception of the sensing coil elements ($\hat{L}_{\mathrm{coil1}}$ and $\hat{L}_{\mathrm{coil2}}$) which contain both δ and $2T$.

The lightwave passes through $\hat{L}_{\mathrm{coil1}}$ and then through the concentrated magnetic field element containing Faraday rotation, $\hat{L}_{F\mathrm{in}}$. It then continues through $\hat{L}_{\mathrm{coil2}}$, strikes the terminating mirror, $\hat{L}_{\mathrm{mirror}}$, and retraces its way back through the optical circuit. To describe the propagation of the oppositely traveling lightwave, we take the transpose of the each Jones matrix, reverse the sign of the off-diagonal elements, and further reverse the sign of the Faraday angle F. This convention preserves a right handed coordinate system with light propagation always to be in the $+z$ direction. This convention accounts for the difference of the two Jones matrices depicting Faraday rotation in the sensing coil, $\hat{L}_{F\mathrm{in}}$ and $\hat{L}_{F\mathrm{out}}$. The composite Jones matrix describing the total light propagation path is summarized in (20)

$$\hat{L}_p = \begin{pmatrix} 1 & 0 \\ 0 & 0 \end{pmatrix} \tag{10}$$

$$\hat{L}_{45°} = \frac{1}{\sqrt{2}}\begin{pmatrix} 1 & -1 \\ 1 & 1 \end{pmatrix} \tag{11}$$

$$\hat{L}_{\mathrm{PMout}} = \begin{pmatrix} 1 & 0 \\ 0 & e^{j(\psi(t)+2\pi\nu\Delta\tau)} \end{pmatrix} \tag{12}$$

$$\hat{L}_{\lambda/4} = \begin{pmatrix} 1 & 0 \\ 0 & e^{-j\frac{\pi}{2}} \end{pmatrix} \tag{13}$$

$$\hat{L}_{\mathrm{coil1}} = \begin{pmatrix} P + jQ & -R \\ R & P - jQ \end{pmatrix} \tag{14}$$

$$\hat{L}_{F\mathrm{out}} = \begin{pmatrix} \cos F & \sin F \\ -\sin F & \cos F \end{pmatrix} \tag{15}$$

$$\hat{L}_{\mathrm{coil2}} = \begin{pmatrix} X + jY & -Z \\ Z & X - jY \end{pmatrix} \tag{16}$$

$$\hat{L}_{\mathrm{mirror}} = \begin{pmatrix} 1 & 0 \\ 0 & -1 \end{pmatrix} \tag{17}$$

$$\hat{L}_{F\mathrm{in}} = \begin{pmatrix} \cos F & -\sin F \\ \sin F & \cos F \end{pmatrix} \tag{18}$$

$$\hat{L}_{\mathrm{PMin}} = \begin{pmatrix} 1 & 0 \\ 0 & e^{j(\psi(t-\tau)+2\pi\nu\Delta\tau)} \end{pmatrix} \tag{19}$$

$$\vec{E}_{\text{out}} = \hat{L}_p \cdot \hat{L}_{45^\circ} \cdot \hat{L}_{\text{PMout}} \cdot \hat{L}_{45^\circ} \cdot \hat{L}_{\lambda/4} \cdot \hat{L}_{\text{coil1}} \cdot \hat{L}_{F\text{out}} \cdot \hat{L}_{\text{coil2}} \cdot \hat{L}_{\text{mirror}} \cdot \hat{L}_{\text{coil2}} \cdot \hat{L}_{F\text{in}} \cdot \hat{L}_{\text{coil1}} \cdot \hat{L}_{\lambda/4} \cdot \hat{L}_{45^\circ} \cdot \hat{L}_{\text{PMin}} \cdot \hat{L}_{45^\circ} \cdot \hat{L}_p \cdot \vec{E}_{\text{in}}. \quad (20)$$

From this output electric field, we calculate the total output light intensity striking the photo-detector of the sensor. Here, we assume a broadband light source and integrate over its frequency spectrum, ν, thus eliminating all terms containing a $\cos 2\pi\nu\Delta\tau$ or $\sin 2\pi\nu\Delta\tau$ dependency. We also define the phase difference modulation, $\Psi_m(t)$, as

$$\Psi_m(t) \equiv \psi(t) - \psi(t-\tau). \quad (21)$$

The output intensity is given by

$$I_{\text{out}} = \langle \vec{E}_{\text{out}} \cdot \vec{E}^*_{\text{out}} \rangle \quad (22)$$

Utilizing sinusoidal modulation, $\Psi_m(t) = \Psi_m \cos\omega t$, together with open-loop demodulation signal processing commonly used for fiber-optic gyroscope applications, the first harmonic component, V_{1H}, of the sensor's output intensity signal is proportional to the Faraday rotation caused by a current

$$V_{1H} = 2I_{\text{in}} \cdot J_1(\Psi_m) \cdot \left\{ [(4QY(-(PX) + RZ)(X^2 - Y^2 + Z^2))] \sin 2F + \left[\left(\frac{1}{2}\right)(P^2 - Q^2 + R^2)^2 (X^2 - Y^2 + Z^2)^2 \right] \sin 4F \right\} \quad (23)$$

where $I_{\text{in}} = \langle |\vec{E}_{\text{in}}|^2 \rangle$.

We assume the usual case that the Faraday induced phase shift is small, $\sin 2F \approx 2F$ and $\sin 4F \approx 4F$. We extract the birefringent dependent coefficient of the local scale factor by normalizing V_{1H} to the light source intensity (I_{in}), the modulation depth ($J_1(\Psi_m)$), and the Faraday rotation ($4F$)

$$\text{SF}_{\text{local}}(\delta, 2T, z) = \frac{V_{1H}}{I_{\text{in}} \cdot J_1(\Psi_m) \cdot 4F}. \quad (24)$$

Replacing the parameters P, Q, R, X, Y, and Z with their representations depicting δ and $2T$, (24) reduces to

$$\text{SF}_{\text{local}}(\delta, 2T, z) = \left(\frac{(2T)^2 + \delta^2 \cos\left(\frac{z}{L}\sqrt{\delta^2 + (2T)^2}\right)}{\delta^2 + (2T)^2} \right) \cdot \left(\frac{(2T)^2 + \delta^2 \cos\left(\sqrt{\delta^2 + (2T)^2}\right)}{\delta^2 + (2T)^2} \right). \quad (25)$$

An inspection of (25) reveals that a z-independent local scale factor is a necessary and sufficient condition to ensure that linear birefringence is not affecting the total scale factor. For the case that the sensing coil contains no circular birefringence ($2T = 0$), the local scale factor along the sensing fiber, $\text{SF}_{\text{local}}(\delta, z)$, varies as the top of a cosine curve (26)

$$\text{SF}_{\text{local}}(\delta, 2T = 0, z) = \cos\left(\delta \frac{z}{L}\right) \cos\delta. \quad (26)$$

The local scale factor, including both linear and circular birefringence (δ and $2T$) in the sensing coil can be stabilized either by reducing δ by annealing the sensing fiber or by adding a large amount of circular birefringence so as to swamp the linear birefringence. $\text{SF}_{\text{local}}(\delta, 2T, z)$ tends to unity for all z, provided $2T \gg \delta$. The fiber may be twisted to achieve a circular birefringence large enough to swamp the linear birefringence, but twisted fiber tends to untwist over time.

It is interesting to note that as $2T$ increases, not only does the maximum deviation from unity decrease, but the periodicity of the variation also increases. Figs. 3–6 show the trend of scale factor variation along the sensing coil for varying amounts of $2T$ for the two cases of an evenly distributed δ of 20 and 40°.

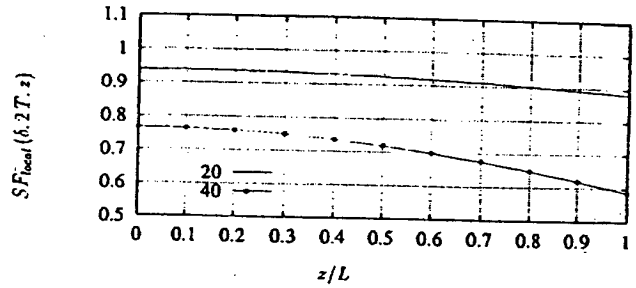

Fig. 3. Scale factor along imperfect sensing coil, $T = 0°$, $\delta = 20°$, and 40°.

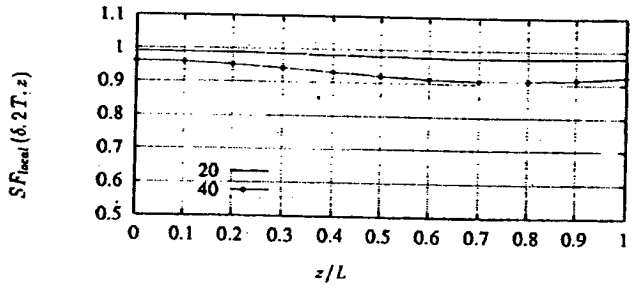

Fig. 4. Scale factor along imperfect sensing coil, $T = 120°$, $\delta = 20°$, and 40°.

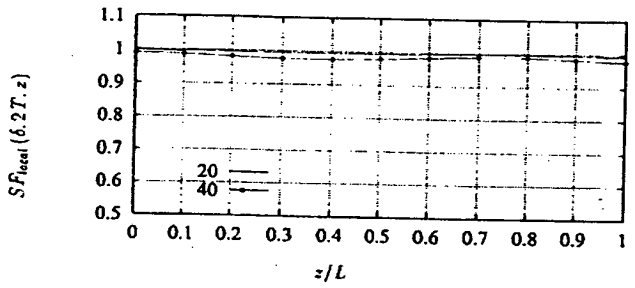

Fig. 5. Scale factor along imperfect sensing coil, $T = 240°$, $\delta = 20°$, and 40°.

IV. Mathematical Modeling of the Overall Scale Factor

A. Open-Loop Signal Processing Configuration

In the open-loop version of the sensor, the birefringence modulator is driven with a sine wave modulation as described

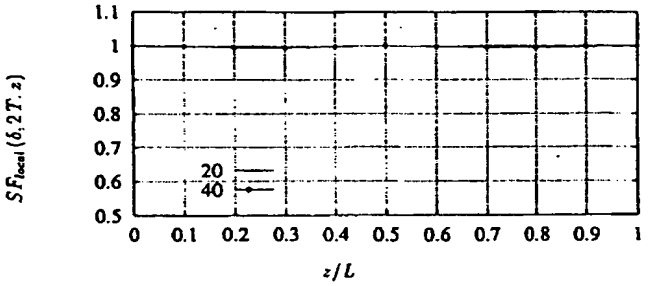

Fig. 6. Scale factor along imperfect sensing coil, $T = 360°$, $\delta = 20°$, and 40°.

above. The first harmonic portion of the signal at the photodetector is taken to be the system output. When the total Faraday induced phase shift is small, the total sensor response may be calculated by integrating the local response of the sensor over its length. Assuming as before that there exists uniformly distributed linear and circular birefringences, (25) may be integrated to obtain the birefringence dependent part of the overall scale factor $\mathrm{SF}(\delta, 2T)$.

$$\begin{aligned}\mathrm{SF}(\delta, 2T) &= \frac{1}{L}\int_0^L \mathrm{SF}_{\mathrm{local}}(\delta, 2T, z)\, dz \\ &= \left(\frac{(2T)^2 + \delta^2 \cos(\sqrt{\delta^2 + (2T)^2})}{\delta^2 + (2T)^2}\right) \\ &\quad \cdot \left(\frac{(2T)^2 + \delta^2\left(\frac{\sin(\sqrt{\delta^2+(2T)^2})}{\sqrt{\delta^2+(2T)^2}}\right)}{\delta^2 + (2T)^2}\right). \end{aligned} \tag{27}$$

A particularly interesting open-loop signal processing scheme for the in-line Sagnac interferometer consists of dividing the first harmonic output by the peak intensity in the detected waveform. This scheme was shown in [8] to desensitize the sensor to imperfections in the quarter-waveplate. The peak output intensity of the current sensor scales with delta and $2T$ as

$$I_{\mathrm{peak}}(\delta, 2T) \propto 1 + \left(\frac{(2T)^2 + \delta^2 \cos(\sqrt{\delta^2 + (2T)^2})}{\delta^2 + (2T)^2}\right)^2. \tag{28}$$

Performing the peak-divide signal processing scheme, the birefringent dependent coefficient of the Faraday rotation scales as dividing (27) by (28)

$$\mathrm{SF}_{\mathrm{peak}}(\delta, 2T) \propto \frac{\mathrm{SF}(\delta, 2T)}{I_{\mathrm{peak}}(\delta, 2T)}. \tag{29}$$

When using the peak divide signal and open-loop processing scheme, the total birefringent dependent scale factor $\mathrm{SF}_{\mathrm{peak}}(\delta, 2T)$ is attenuated in the presence of linear birefringence, δ, in the sensing coil. However, as circular birefringence, $2T$ is added, the scale factor error may be eliminated. Fig. 7 show the birefringent dependent scale factor as a function of $2T$ for $\delta = 20°$ and 40°. As very large amounts of $2T$ are added, the scale factor error is effectively reduced to zero.

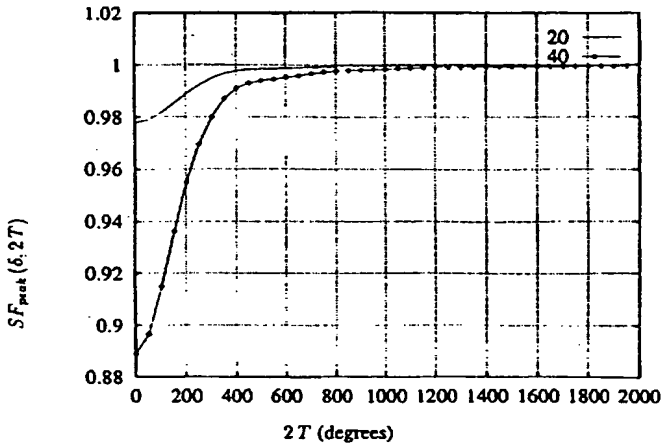

Fig. 7. Scale factor as a function of $2T$, $\delta = 20°$ and 40°.

In the absence of circular birefringence in the sensing coil ($2T = 0$), the scale factor dependence, as a function of δ, is given as

$$\begin{aligned}\mathrm{SF}(\delta, 2T = 0) &= \frac{1}{L}\int_0^L \mathrm{SF}_{\mathrm{local}}(\delta, 2T = 0, z)\, dz \\ &= \frac{\sin 2\delta}{2\delta}. \end{aligned} \tag{30}$$

The dependence of the scale factor on linear birefringence when employing the peak divide signal processing scheme, $\mathrm{SF}_{\mathrm{peak}}(\delta, 2T = 0)$, is given below. Even in the absence of any linear birefringence compensation, the peak divide signal processing scheme does provide some scale factor error reduction (compare Figs. 7 and 8).

$$\mathrm{SF}_{\mathrm{peak}}(\delta, 2T = 0) \propto \frac{\mathrm{SF}(\delta, 2T = 0)}{I_{\mathrm{peak}}(\delta, 2T = 0)} \propto \frac{\left(\frac{\sin 2\delta}{2\delta}\right)}{1 + \cos^2 \delta}. \tag{31}$$

Linear birefringence within the sensing coil near the quarter-waveplate ($\lambda/4$) may simply be taken as an error in the $\lambda/4$ itself, and is therefore compensated by the peak divide signal processing. However, linear birefringence existing further within the sensing coil yields an error that is not completely compensated by this signal processing. Thus the desirability of adding circular birefringence or eliminating the linear birefringence in the sensing coil remains.

B. Closed-Loop Signal Processing Configuration

Similar to the fiber-optic gyroscope, the in-line Sagnac interferometer current sensor may be operated "closed loop." A Ti-indiffused $LiNbO_3$ integrated optics straight waveguide modulator is used to provide the birefringence modulation. A phase ramp waveform is added to the usual periodic waveform for providing a nonreciprocal phase shift equal and opposite to the Faraday induced phase shift. The first harmonic, V_{1H} of the periodic waveform is thereby nulled in the sensor output.

The Jones matrix modeling of the closed-loop sensor is the same as the open-loop sensor with the one exception that (12)

is changed to

$$\hat{L}_{\text{PM out}} = \begin{pmatrix} 1 & 0 \\ 0 & e^{j(\psi(t)+2\pi\nu\Delta\tau+\gamma_0(\delta,2T,F,z))} \end{pmatrix} \tag{32}$$

Here, $\gamma_0(\delta, 2T, F, z)$ represents the effective nonreciprocal phase shift that is added to the system by the birefringence modulator. After performing the Jones matrix analysis, the phase shift γ_0 which is required to zero V_{1H} is given below as a function of linear birefringence, δ, circular birefringence, $2T$, Faraday rotation F and position along the sensing coil z.

$$\gamma_0(\delta, 2T, F, z) = -2\tan^{-1}\left(\tan 2F \cdot \left(\frac{(2T)^2 + \delta^2\cos\left(\frac{z}{L}\sqrt{\delta^2+(2T)^2}\right)}{(2T)^2+\delta^2\cos\left(\sqrt{\delta^2+(2T)^2}\right)}\right)\right). \tag{33}$$

It is evident from (33) that a z-independent local scale factor is again a necessary and sufficient condition to ensure that there is no adverse effect of linear birefringence on the sensor. As with the open-loop case, this condition is satisfied when $2T \gg \delta$.

To calculate the total phase shift which must be induced to zero V_{1H} we perform a similar mathematical analysis which does not assume a localized magnetic field $\vec{H}$, but rather assumes an evenly distributed magnetic field along the entire length of the sensing coil. For the closed-loop signal processing configuration, it is not appropriate simply to integrate the localized phase shift $\gamma_0(\delta, 2T, F, z)$ with respect to z to find the total phase shift $\gamma_0(\delta, 2T, F)$ required to zero V_{1H}. The principle which allows the total scale factor to be derived by integrating the localized scale factor in the open-loop signal processing configuration is the fact that a linear sensor response is assumed. For the closed-loop case, which can handle much larger values of Faraday rotation, the assumption of a small Faraday angular rotation should not be pressed.

The resultant total phase shift required to zero V_{1H} in the closed-loop signal processing approach is given in (34), and the closed-loop birefringent dependent coefficient $\text{SF}_{\text{cl}}(\delta, 2T)$ given in (35) is shown in Fig. 8

$$\gamma_0(\delta, 2T, F) = (-4F)\cdot\left(\frac{(2T)^2+\delta^2\left(\frac{\sin\left(\sqrt{\delta^2+(2T)^2}\right)}{\sqrt{\delta^2+(2T)^2}}\right)}{(2T)^2+\delta^2\cos\left(\sqrt{\delta^2+(2T)^2}\right)}\right) \tag{34}$$

$$\text{SF}_{\text{cl}}(\delta, 2T) = \frac{\gamma_0(\delta, 2T, F)}{-4F}. \tag{35}$$

An interesting aspect of the closed-loop system is that the error has several zero crossings (Fig. 8) irrespective of the amount of total δ in the sensing coil (assuming $2T > \delta$). Precise and exact amounts of $2T$ may be introduced to any sensing coil, regardless of its given δ and the scale factor error associated with δ can be completely overcome. The unity crossings of $\gamma_0(\delta, 2T, F)$ (Fig. 8) are given below.

$$\tan 2T = 2T. \tag{36}$$

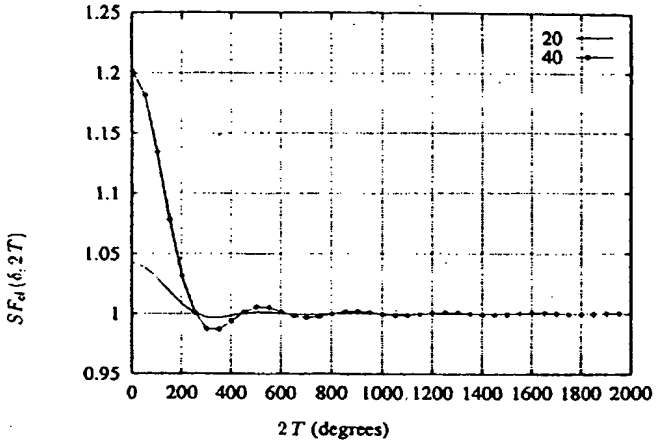

Fig. 8. Scale factor as a function of $2T$, $\delta = 20°$ and $40°$.

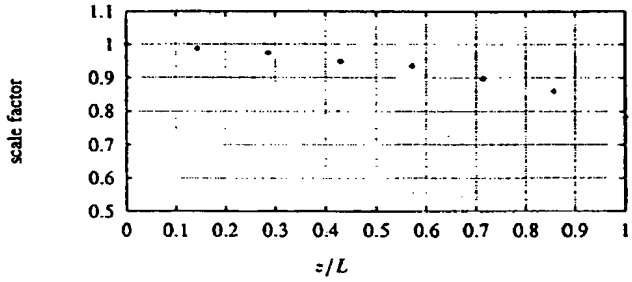

Fig. 9. Scale factor with no applied twist.

However, as can be seen by Fig. 8, as the total amount of $2T$ continues to increase, the error in the scale factor becomes negligible. A more robust solution is to induce as much circular birefringence as possible.

V. Experimental Results

A. Straight Sensing Coil

We first performed an experimental analysis of the setup shown in Fig. 2. To apply a localized magnetic field $\vec{H}$ along the sensing coil, we used a very small air core inductor and mapped the magnitude of the scale factor as we moved the inductor along the sensing coil. For this series of tests, we simply twisted the fiber to induce $2T$. The experimental results (Figs. 9–11) are seen to follow qualitatively the predicted behavior as shown in Figs. 3–6.

Fig. 9 shows the scale factor response along the length of the sensing coil (one meter long) in the specific case of no circular birefringence, i.e., $2T = 0$. Clearly the scale factor drops off as the top of a cosine curve. Fig. 10 shows the scale factor response along the length of the sensing coil when the entire length of the sensing coil has undergone a moderate amount of twisting. Its behavior resembles that shown in Figs. 4–5 for the oscillatory effect as well as decreased deviation from unity of the scale factor. Fig. 11 shows the scale factor response when a very large amount of twisting had been applied to the sensing coil. For this case, a large amount of $2T$ has been introduced,

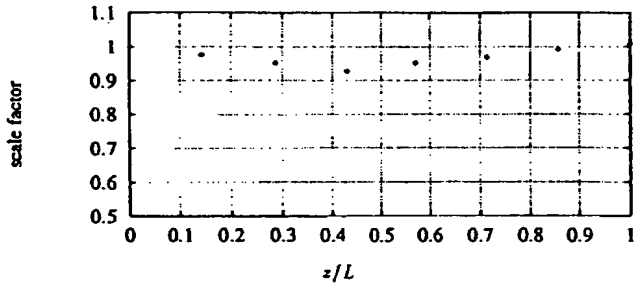

Fig. 10. Scale factor with a moderate applied twist (840°).

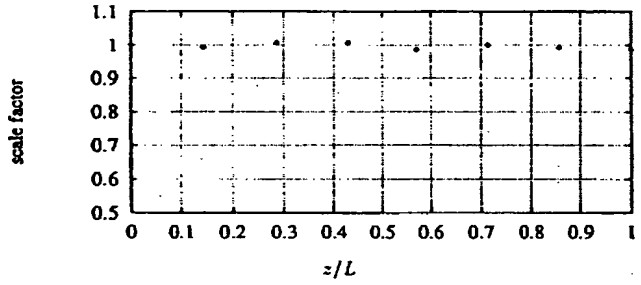

Fig. 11. Scale factor with a large applied twist (3120°).

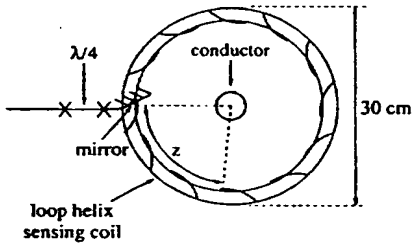

Fig. 12. Loop helix sensing coil geometry and setup.

and the scale factor is approximately constant all along the sensing coil.

B. Loop Helix Sensing Coil

An alternative way to add a large amount of circular birefringence to the sensing coil is to wind it in a helix [11], as shown in Fig. 12. This method of adding circular birefringence is much more robust than twisting the fiber, as the circular birefringence is the result of the geometrical torsion, and therefore does not change with temperature and time. For our laboratory experiment testing this particular implementation of the sensing coil, our setup included a loop helix sensing coil wound with a sensing coil radius of approximately 30 cm. Our helix contained twelve complete rotations evenly distributed around the sensing coil. The radius of our helix is approximately 5 mm.

In this configuration, the sensing coil undergoes an incremental change of coordinate axes all along its length, provided there exist well defined axes of linear birefringence oriented parallel and perpendicular to the plane of the fiber bending. To ensure that the sensing coil contains well-defined δ axes which

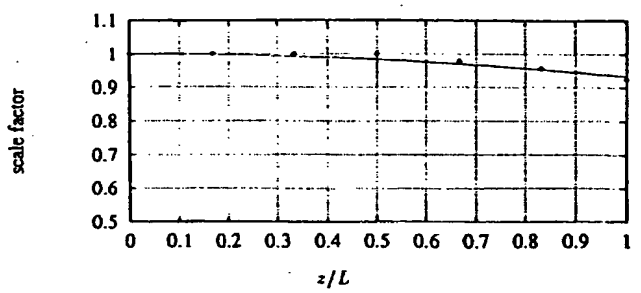

Fig. 13. Scale factor along loop helix sensing coil (no axial strain); the curve fit uses $\cos(\delta z/L)$ with $\delta = 21°$.

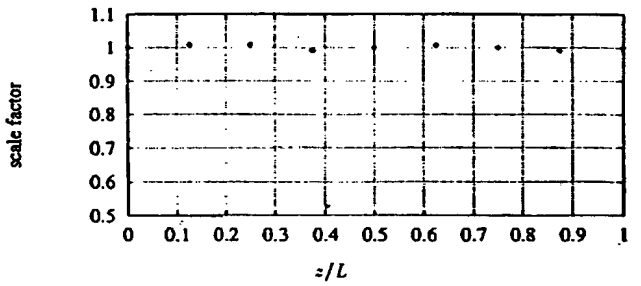

Fig. 14. Scale factor along loop helix sensing coil (with axial strain).

follow the geometrical twist along the helix, the sensing coil should be held with some axial tension. Unless the sensing coil is very small, the bend birefringence is not typically large enough to overcome the intrinsic birefringence built into the fiber. However, bending with a small amount of axial strain does provide sufficient linear birefringence to define a rotating coordinate system.

Figs. 13 and 14 show experimental confirmation that winding the sensing fiber in a helix and adding axial strain stabilizes the scale factor along the sensing loop. A localized magnetic field was induced using a small air-core inductor around the sensing fiber. When the helically wound fiber was loose, the cosine dependence of the scale factor along the length of the sensing fiber is evident as shown in Fig. 13. Then, when a small amount of tension was added to the helically wound fiber, the scale factor straightened out as shown in Fig. 14.

VI. Conclusion

We have performed a mathematical analysis of scale factor error associated with linear birefringence δ in the sensing coil of the in-line Sagnac interferometer current sensor. In doing this, we found the spatial dependence of the scale factor along the sensing coil of the current sensor as well as the total scale factor of the current sensor as a function of both linear and circular birefringence (δ and $2T$) in the sensing coil.

We achieved experimental verification of this spatial scale factor dependence along a sensing coil containing varying amounts of δ and $2T$. In doing so, we showed that the scale factor error of a sensing coil containing sufficiently large amounts of $2T$ may be effectively eliminated. We achieved a flat scale factor result experimentally, and we are therefore assured that our sensing coil is free from any linear

birefringence induced uncertainties. The use of a helically wound sensing coil under modest tension was shown to desensitize the sensor to intrinsic linear birefringence built into the sensing fiber. We believe this design obviates the need for the use of annealed fiber in the sensing coil.

ACKNOWLEDGMENT

The authors thank Dr. M. Messerley at 3M Corporation, St. Paul, MN, B. Szafraniec at Honeywell, Inc., Phoenix, AZ, and Dr. R. Dyott at Andrew Corporation, Orland Park, IL, for providing optical fiber used in this work.

REFERENCES

[1] E. Shafir, N. Shaked, A. Ben-Kish, and M. Tur, "The response of Faraday-effect fiber-optic current sensors to noncentered currents," in *Proc. 9th Int. Conf. Optic. Fiber Sensors*, IEEE, New York, 1993, pp. 435–438.

[2] T. W. MacDougall and T. F. Hutchinson, "Stray magnetic-field response of linear birefringent current sensors," *Appl. Opt.*, vol. 34, no. 21, pp. 4373–4379, 1995.

[3] J. Blake, P. Tantaswadi, and R. T. de Carvalho, "In-line Sagnac interferometer for magnetic field sensing," in *Proc. 10th Int. Conf. Optic. Fiber Sensors (OFS-10), Proc. SPIE 2360*, B. Culshaw and J. D. C. Jones, Eds., 1994, pp. 419–422.

[4] J. Blake, P. Tantaswadi, and R. T. de Carvalho, "In-line Sagnac interferometer current sensor," *IEEE Trans. Power Delivery*, vol. 11, no. 1, pp. 116–121, 1996.

[5] G. Frosio and R. Dändliker, "Reciprocal reflection interferometer for a fiber-optic faraday current sensor," *Appl. Opt.*, vol. 33, no. 25, pp. 6111–6122, 1994.

[6] S. X. Short, P. Tantaswadi, R. T. de Carvalho, B. D. Russell, and J. Blake, "An experimental study of acoustic vibration effects in optical fiber current sensors," *IEEE Trans. Power Delivery*, vol. 11, no. 4, pp. 1702–1706, 1996.

[7] S. X. Short, P. Tantaswadi, R. T. de Carvalho, B. D. Russell, and J. Blake, "Environmental sensitivity comparison of in-line sagnac and polarimetric type current sensors," in *Proc. 11th Int. Conf. Optic. Fiber Sensors (OFS-11), Japan Soc. Appl. Phys.*, 1996, pp. 276–279.

[8] S. X. Short, A. A. Tselikov, J. U. de Arruda, and J. Blake, "Imperfect quarter-waveplate compensation in Sagnac interferometer type current sensors," *J. Lightwave Technol.*, vol. 16, pp. 1212–1219, July 1998.

[9] D. Tang, A. H. Rose, G. W. Day, and S. M. Etzel, "Annealing of linear birefringence in single-mode fiber coils: Application to optical fiber current sensors," *J. Lightwave Technol.*, vol. 9, Aug. 1991.

[10] K. Kurosawa and I. Masuda, "Faraday effect current sensor using flint glass fiber for the sensing element," in *Proc. 9th Int. Conf. Optic. Fiber Sensors*, IEEE, New York, 1993, pp. 415–418.

[11] F. Maystre and A. Bertholds, "Magneto-optic current sensor using a helical fiber fabry-perot resonator," in *Proc. 6th Int. Conf. Optic. Fiber Sensors (OFS-6), Springer Proceedings in Physics*, 1989, vol. 44, pp. 267–272.

Shayne X. Short was born in Billings, MN, in 1971. He received the B.S., M.S., and Ph.D. degrees in electrical engineering from Texas A&M University, College Station, in May 1993, May 1995, and August 1997, respectively.

His graduate studies in Electrical Engineering at Texas A&M University focused on fiber-optic current sensors designed primarily for electric power system applications. He is presently enrolled at the University of Texas School of Law, Austin, from which he anticipates a May 2000 graduation. Additionally, he is presently a Technical Advisor for the law firm of Akin, Gump, Strauss, Hauer and Feld, L.L.P., Austin, TX.

Dr. Short is recipient of the 1992 IEEE PES T. Burke Hayes Award and a 1994 IEEE Vincent Bendix Award. He is a member of the Eta Kappa Nu, Tau Beta Pi, Phi Kappa Phi, and Golden Key honor societies.

Josiel U. de Arruda was born in Araraquara, São Paulo, Brazil, in 1961. He received the B.S. and M.S. degrees in electronics engineering from the Instituto Tecnológico de Aeronáutica, São José dos Campos, São Paulo, Brazil, in 1987 and 1994, respectively. He is currently working towards the Ph.D. degree in electrical engineering at Texas A&M University, College Station, sponsored by the Brazilian Air Force.

From 1988 to 1994, he was a Researcher at the Instituto de Estudos Avançados (IEAv), Centro Técnico Aeroespacial, São José dos Campos, São Paulo, Brazil. His technical fields of interest include fiber-optic sensors and related signal processing issues.

Alexandr A. Tselikov was born in Kuibushev, Russia, in 1967. He received the B.S. and M.S. degrees in physics and engineering from Moscow Engineering Physics Institute, Russia, in 1990 and the Ph.D. degree in electrical engineering from Texas A&M University, College Station, in 1998.

From 1990 to 1994, he worked at the Lebedev Physics Institute for the Frequency Standard Laboratory, Moscow, Russia. From 1994 to 1995, he helped to develop a transportable diode laser frequency standard at the Physikalish Technishe Bundesanschtalt, Braunschweig, Germany. He is currently with Quinta, a Seagate company, San Jose, CA, working on the development of a new type of magneto-optical data storage system. His technical fields of interest include optical fiber devices, signal processing, analog electronics design, semiconductor laser physics, and magneto-optical data storage systems.

James N. Blake was born in Oakland, CA, in 1959. He received the B.S. degree in electrical engineering from the University of California, Berkeley, in 1981 and the Ph.D. degree from Stanford University, Stanford, CA, in 1988, where he pioneered two-mode fiber-strain sensors and frequency shifters.

From 1981 to 1984, he was a Microwave Engineer at Ford Aerospace, Palo Alto, CA. From 1988 to 1991, he was the Technical Leader of the group that developed the world's first commercial fiber-optic gyroscope product at Honeywell's Systems and Research Center, Phoenix, AZ. In 1991, he joined the Faculty at Texas A&M University, where he is continuing research in the area of Sagnac interferometry. He has over 60 technical publications and 12 issued patents.